Elastic and inelastic scattering of ^{16}O from ^{20}Ne

M. Gai,* G. M. Berkowitz,† P. Braun-Munzinger, C. M. Jachcinski,‡ C. E. Ordoñez,§ T. R. Renner,** and C. D. Uhlhorn††
Department of Physics, State University of New York at Stony Brook, Stony Brook, New York 11794
(Received 19 March 1984)

A differentially pumped gas cell was used to study the angular and energy dependence of elastic and inelastic scattering of ^{16}O from ^{20}Ne. The data exhibit the characteristic features of gross and intermediate structures observed previously for lighter systems. The slopes of the measured angular distributions show rapid variations as a function of energy and a strong rise toward backward angles. The data are discussed in terms of α-particle exchange, resonances, and statistical fluctuations.

I. INTRODUCTION

Reactions between $0p$-shell nuclei like $^{12}C+^{12}C$ or $^{16}O+^{16}O$ are characterized[1] by strongly energy dependent structures which can be classified according to their width. For example, in the elastic scattering excitation function of the system $^{16}O+^{16}O$, three different types of structures are identified[2,3] with widths of $\Gamma \approx 100$ keV (fine structure), $\Gamma \approx 100$–500 keV (intermediate structure), and $\Gamma \approx 2$–3 MeV (gross structure). In other systems this separation is not so obvious and, in particular, the distinction between fine and intermediate structures is often lost. While the fine structure (if it can be identified) is generally explained in terms of statistical fluctuations,[4] no agreement exists up to now as to the origin of the gross and intermediate structures. Isolated or overlapping resonances, exchange effects, and strong coupling of inelastic channels have been invoked to understand the intermediate structure, while shape resonances or angular momentum matching conditions explain equally well the observed gross structure. A complete summary of the data can be found in Refs. 1 and 5.

Quite recently, it was observed[6,7] that similar gross and fine structures persist for much heavier systems such as $^{16}O+^{28}Si$, $^{12}C+^{28}Si$, and even $^{28}Si+^{28}Si$ (Ref. 8), thereby indicating that these energy dependent structures are a phenomenon of much wider range than previously believed. In order to explore experimentally the region in between the heavy and light systems, we have investigated the energy dependence of elastic and inelastic scattering for the system $^{16}O+^{20}Ne$. This system is also interesting because the small α threshold in ^{20}Ne should enhance possible effects due to the exchange of identical ^{16}O cores.

In Sec. II, the experimental method is described. Section III contains a description of the experimental data. Implications of these data and various relevant models are discussed in Sec. IV.

II. EXPERIMENTAL METHOD

Data were taken using ^{16}O beams of the Stony Brook FN tandem Van de Graaff accelerator. A windowless, differentially pumped gas cell described in detail in the following was used as a ^{20}Ne target. Scattered ^{16}O and recoiling ^{20}Ne ions were identified and their energies measured in three ΔE-E ionization chamber telescopes of the Berkeley design.[9] Typical energy spectra for both Ne and O ions are shown in Fig. 1. From this figure it is evident that the obtained energy resolution of $\delta E \leq 600$ keV was sufficient to resolve completely the transitions to the ground and first excited states in ^{20}Ne. The target consisted of ^{20}Ne gas enriched to 99.9%.

In Fig. 2 is shown a schematic diagram of the differentially pumped gas cell and the gas recycling system used in the present experiments. The beam enters the gas cell after passing through three sets of collimators of 1.5–2.5 mm diameter. Using a Roots blower and a turbo molecular pump, both backed by sealed mechanical pumps, a very large pressure gradient can be maintained between the inside of the gas cell and the scattering chamber. For example, for a pressure of 30 Torr in the gas cell measured at point A (see Fig. 2), the pressure at the Roots blower inlet (point B) is ~ 0.5 Torr and the pressure at the turbo pump inlet (point C) is $\sim 4\times 10^{-3}$ Torr. At the same time the pressure in the scattering chamber (point D) can be maintained below 1.5×10^{-5} Torr. For the present gas cell the ^{20}Ne gas target has an areal density of $\sim 40\ \mu g/cm^2$ at a gas pressure of 35 Torr. The gas pumped by the Roots blower and turbo pump was cleaned from oil contamination in various cold traps kept at $-30°$ C, or at liquid nitrogen temperature and in a molecular sieve and fed back into the gas cell via an automatic pressure controller. Typical flow rates were of the order of 20 standard cm^3/s. The gas flow exiting through the entrance aperture is, under those conditions, approximately 5×10^{-4} standard cm^3/s. In this recycling mode the pressure in the cell could be kept constant to within ~ 0.5 Torr over a period of several days. To check for purity, the gas was periodically analyzed on line using a mass spectrometer. To eliminate buildup of small contaminations the gas was purged about every 24 h.

The beam passes through 3.5 cm of gas at the effective gas cell pressure before entering the active area of the cell. Scattered particles travel through ~ 2.5 cm of gas and exit the cell through a stretched polypropylene foil of $\sim 75\ \mu g/cm^2$ areal density. A thin pinhole-free Ni foil ($0.4\ mg/cm^2$) served as the exit foil for the beam.

The excitation function data were normalized to the

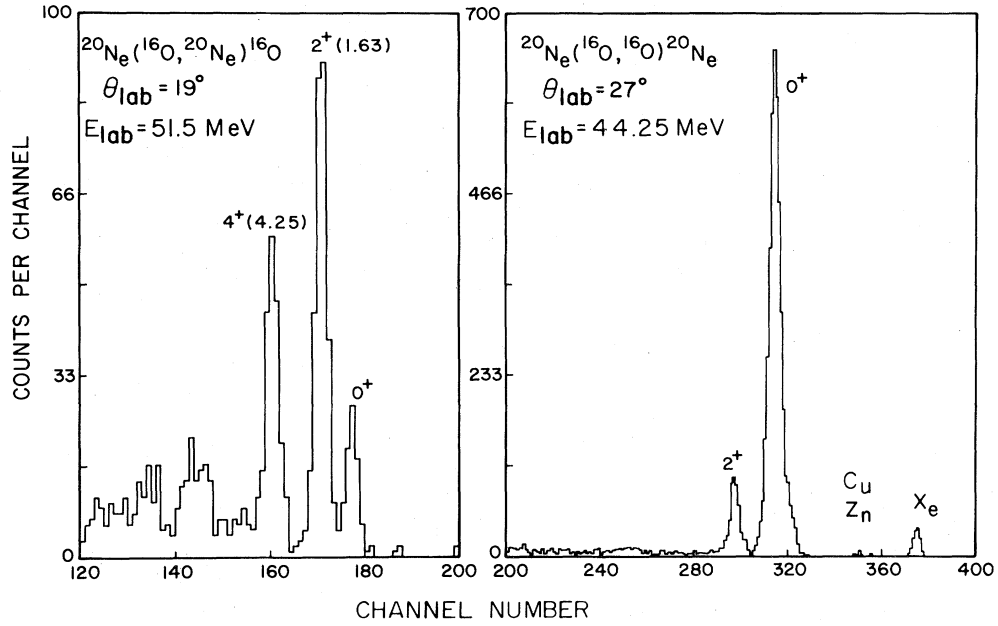

FIG. 1. Typical spectra of scattered and recoil ions from a ^{16}O beam and ^{20}Ne gas target.

Rutherford scattering of the ^{16}O ions off the Ni exit foil and by using the integrated beam current. The absolute cross section was established by measuring the elastic excitation functions down to very low energies where the cross section follows the Rutherford law at all angles. The relative accuracy of the excitation function data is essentially determined by statistical errors. The accuracy of the absolute cross section is about $\pm 20\%$.

For the angular distribution measurements, the dependence in scattering angle of the effective target thickness and solid angle was determined by filling the cell with about 5 Torr of pure Xe and measuring Rutherford scattering of ^{16}O from Xe. The overall accuracy of the relative normalization of the angular distribution data is believed to be better than 20%, except for the angular range $90° \leq \theta_{c.m.} \leq 130°$, where $\delta\sigma/\sigma \leq \pm 35\%$.

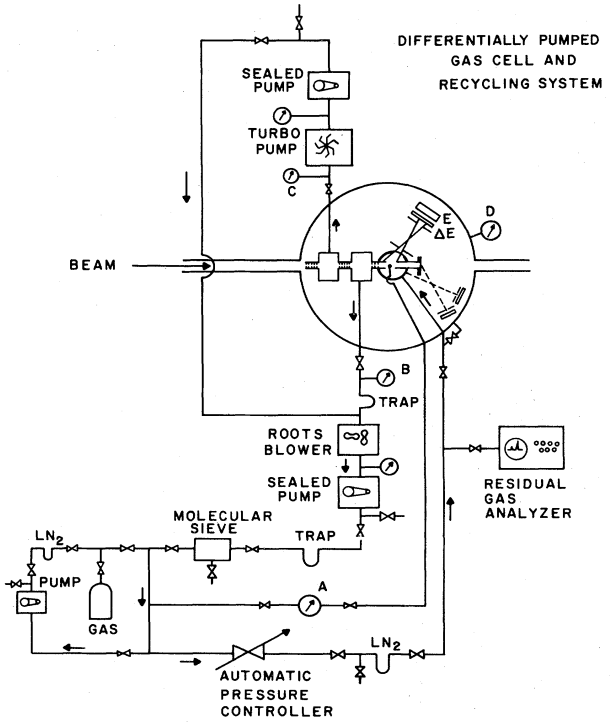

FIG. 2. Schematic diagram of the differentially pumped gas cell and the gas recycling system.

III. EXPERIMENTAL RESULTS

Excitation functions were studied at backward angles for elastic and inelastic scattering of ^{16}O from ^{20}Ne. The cell pressure was varied between $15 \leq P \leq 35$ Torr depending on beam energy to yield energy averaging of $\Delta E_{lab} \sim 250$ keV. Hence, the step size was $200 \leq \delta E_{lab} \leq 300$ keV. Beam energies were corrected for energy loss and transformed to the center of mass system. Complete excitation functions were measured for the recoil particles at $\theta_{lab}=17°$ and 27° for $9 \leq E_{c.m.} \leq 30$ MeV. The excitation functions for three exit channels schematically labeled at 0^+, 2^+, and 4^+ for $\theta_{lab}=17°$, 22°, 25°, 27°, 32°, and 35° are shown in Figs. 3–5.

All studied excitation functions exhibit a gross oscillatory pattern ($\Gamma \sim 2$ MeV) modified by a structure of intermediate width ($\Gamma \leq 500$ keV). Some degree of correlation is found between excitation functions of different channels at different angles. The high energy part of the data presented here is generally in good agreement with independent measurements of $^{16}O+^{20}Ne$ at high energies.[10,11] General overall correlation with structure observed[10,12] in the reaction channel $^{20}Ne(^{16}O,^{12}C)^{24}Mg$ is also found. We note, however, that a pronounced structure at $E_{c.m.} \approx 18$ MeV is observed in all four angles in

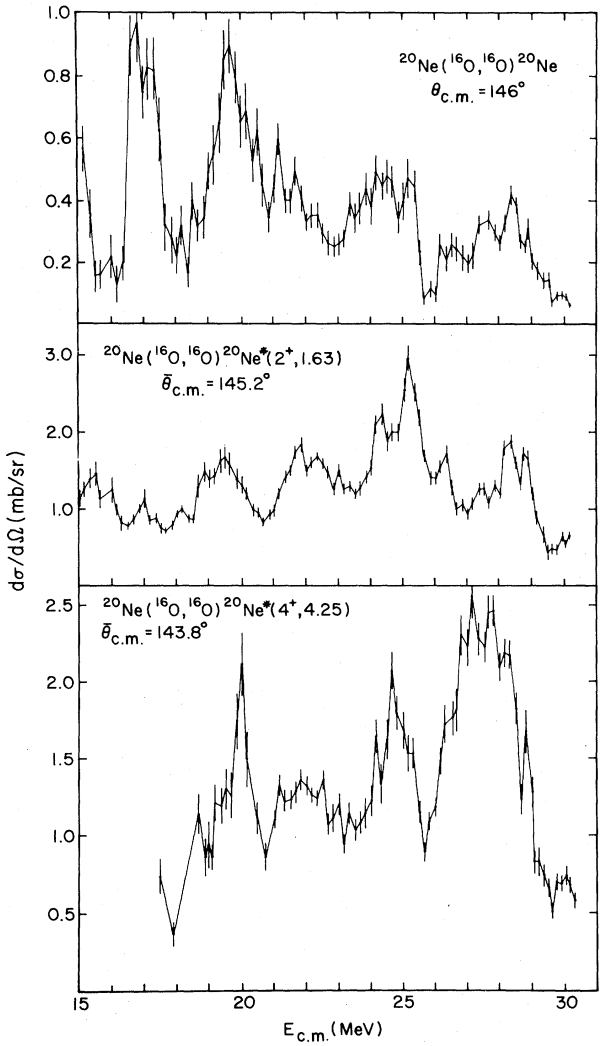

FIG. 3. Excitation functions for the scattering of ^{16}O off ^{20}Ne at $\theta_{lab}=17°$ in three exit channels. The measurements at $E_{c.m.} \leq 21$ MeV were performed at a gas pressure of $p=15$ Torr and at $p=35$ Torr for the higher energies.

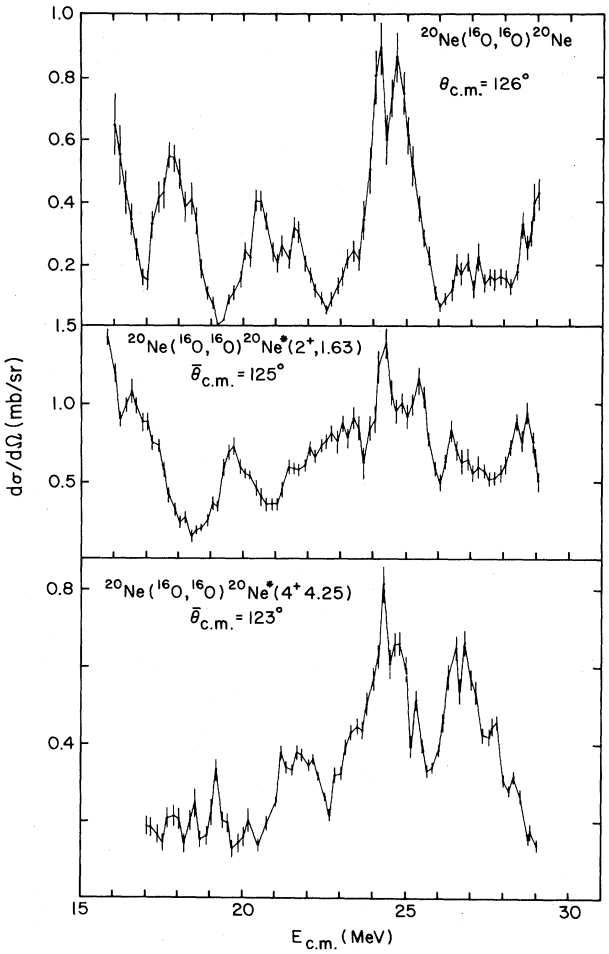

FIG. 4. As for Fig. 3, at $\theta_{lab}=27°$.

the elastic channel, but not in any of the inelastic channels (see Fig. 4). It was noted[13] that such structures characteristically appear in many heavy ion systems right above the barrier. Such structures are now under continuing investigation by the authors of Ref. 13. A pronounced structure is also observed at $E_{c.m.} \approx 24.5$ MeV in all channels. This structure appears in the total reaction cross section measured with gamma ray techniques.[14] In our study we thus concentrated on these two structures near 18 and 24.5 MeV.

Angular distributions were measured in the angular range $27° \leq \theta_{c.m.} \leq 150°$ in steps of $1° \leq \delta\theta_{c.m.} \leq 2°$. The elastic scattering angular distributions are shown in Fig. 6, and in Fig. 7 we show the angular distributions for inelastic scattering ($Q=-1.63$ MeV) to the first excited 2^+ state of ^{20}Ne. Generally good agreement is found for angular distributions measured independently with gas and solid targets.[10,11,15,16]

All inelastic scattering angular distributions are rather structureless (see Fig. 7). The angular distributions of the elastic channel at the region above the Coulomb barrier show oscillatory behavior at large backward angles and a sharp diffractive type of dropoff at forward angles. It is interesting to note that the two angular distributions at $E_{c.m.}=24.2$ and 24.7 MeV are similar in the backward angles region ($\theta_{c.m.} \geq 105°$) and in the forward angles region ($\theta_{c.m.} \leq 65°$). However, marked differences between the two angular distributions at the intermediate angles region can be seen in Fig. 6. For the angular distribution at $E_{c.m.}=17.4$ and 18.5 MeV we note that while the first one shows regular oscillatory behavior at backward angles, the second angular distribution is nearly flat for $\theta_{c.m.} < 120°$. The significance of these four angular distributions is discussed in Sec. IV.

IV. DISCUSSION

A. Statistical analysis

In order to test the validity of a possible resonance interpretation we have studied the degree of correlation between the different excitation functions measured at dif-

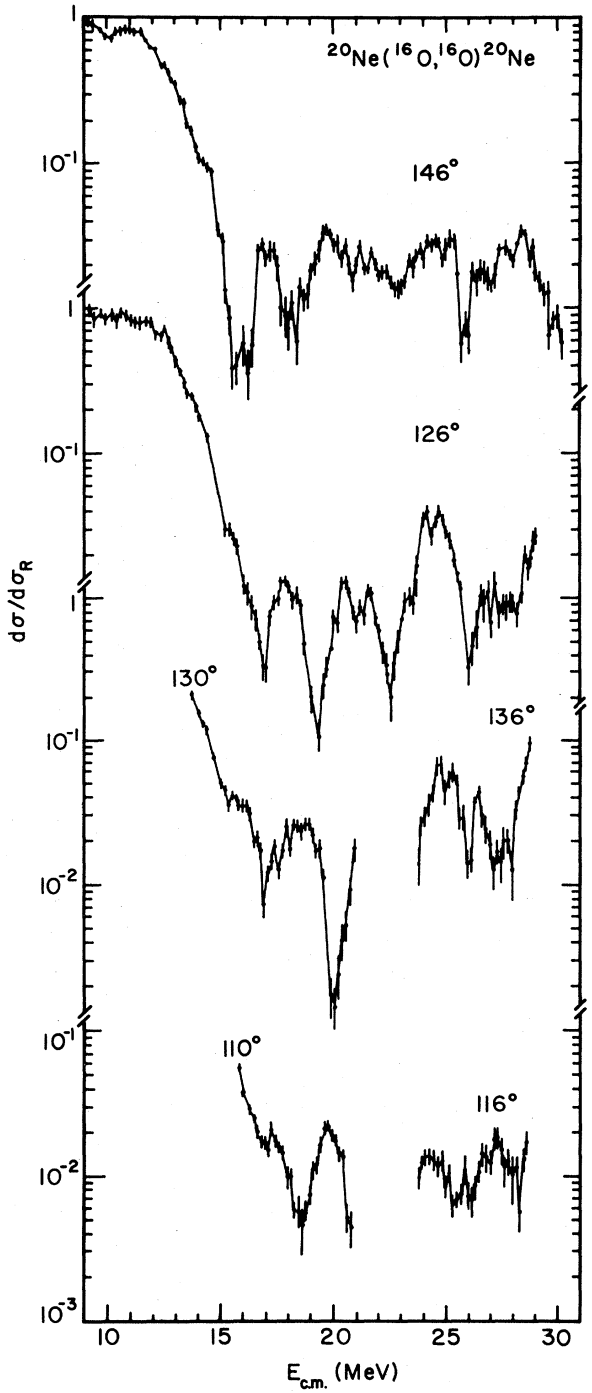

FIG. 5. Elastic scattering excitation functions for the $^{16}O+^{20}Ne$ system at four different angles.

ferent angles. Such correlation can be established by studying the symmetrized correlation function,[17] defined as

$$C_{ij}^{\Delta}(\epsilon)=\frac{1}{2}\left\{\frac{\langle d_i(E)d_j(E+\epsilon)\rangle}{[\langle d_i(E)^2\rangle\langle d_j(E+\epsilon)^2\rangle]^{1/2}}+\frac{\langle d_i(E+\epsilon)d_j(E)\rangle}{[\langle d_i(E+\epsilon)^2\rangle\langle d_j(E)^2\rangle]^{1/2}}\right\}, \quad (1)$$

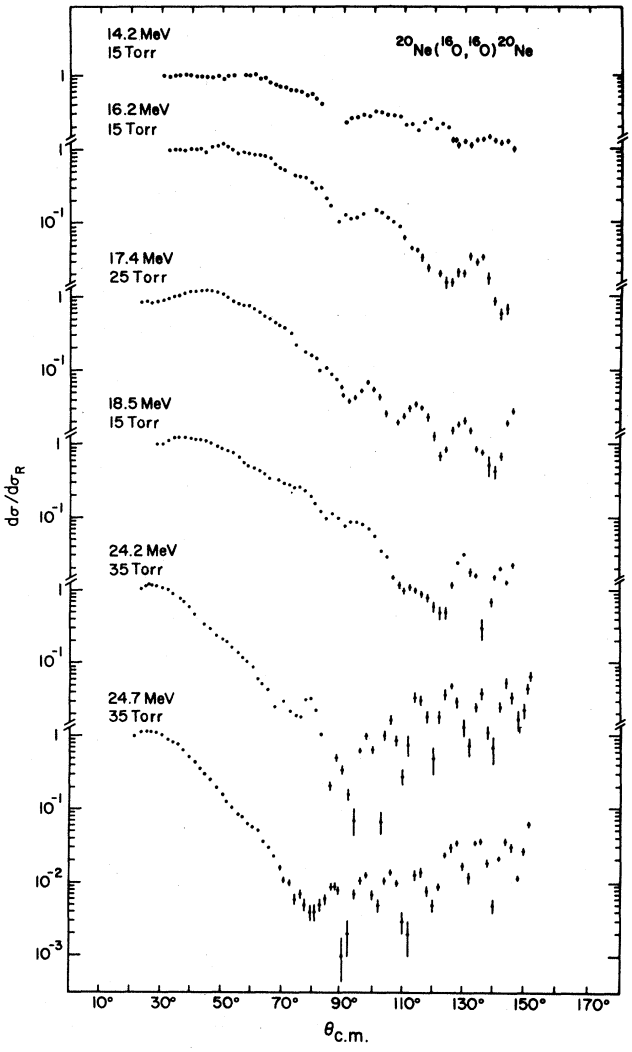

FIG. 6. Elastic scattering angular distribution measured in the vicinity of maxima of the elastic scattering excitation function. At intermediate angles the normalization is good to within ±35%.

with

$$d_i(E)=\frac{\sigma_i(E)}{\langle\sigma_i(E)\rangle_{\Delta}}-1\,,$$

where the bracket $\langle\ \rangle$ denotes averaging over the full interval and $\langle\ \rangle_{\Delta}$ denotes averaging using a Gaussian weight distribution with width Δ. The Gaussian width (Δ) has to be chosen to be smaller than the width of the "gross structure" but larger than the width of the "intermediate structure." Of course, these requirements, in some cases, are conflicting. Two fully correlated (anticorrelated) functions will have a cross correlation coefficient of 1 (-1). In the simple statistical model,[18] two channels ($i\neq j$) will have a zero cross correlation coefficient ($C_{ij}=0$). A more sophisticated statistical model which takes direct background amplitudes into account[19] allows two different channels to have nonvanishing cross correla-

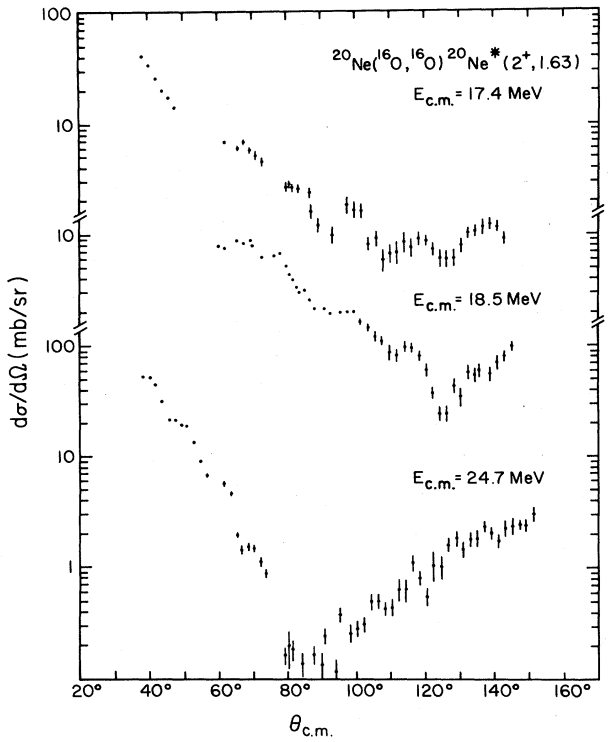

FIG. 7. Inelastic scattering angular distributions.

tions. We performed channel-channel and angular cross correlation studies for the three channels: elastic and inelastic ($Q=-1.6$ and -4.2 MeV) measured at $\theta_{lab}=17°$ and 27°. The dependence of $C_{ij}(0)$ on Δ was studied and it was found that around $\Delta\simeq 1.2$ MeV the correlation functions are insensitive to variations in Δ. Linear interpolation between data points was done whenever necessary. Artificial extension of the data below and above the measured region was carried out. The finite range of the data yields an error in the value of the estimated cross correlations.[4] The correlation coefficients are given in Table I and the finite range of data error is given, too.

As can be seen from Table I, the excitation functions measured at $\theta_{lab}=17°$ exhibit a fairly large degree of channel-channel cross correlation for all three measured channels. However, poor cross correlation results are obtained for $\theta_{lab}=27°$. Furthermore, a significant degree of correlation is observed between the inelastic channel of $Q=-1.6$ MeV measured at $\theta_{lab}=27°$ and all scattering channels measured at $\theta_{lab}=17°$. The overall degree of correlation appears to be significant; five correlation coefficients have values which are five standard deviations from zero, and, for the rest, only four are within one standard deviation of zero. Some particular structures, such as that at 24.5 MeV, are clearly observed at all angles and in all channels, suggesting a resonance character.

B. Optical model and resonance(s)

In this scheme one explicitly adds a Breit-Wigner resonance term to a smooth background amplitude calculated from a (strongly absorbing) optical model. Explicitly introducing a resonance yields, for the nuclear part of the elastic scattering S matrix for spinless particles,

$$S=S^{OM}+S^{res},$$
$$S^{res}=-e^{2i(\delta_{OM}+\phi)}\frac{iD}{E-E_R+i\Gamma/2}\delta_{l,l_R}, \tag{2}$$

where δ_{OM} is the optical model background phase shift, D is the partial elastic width, Γ is the total width, ϕ is a resonance mixing phase, and E_R is the resonance energy. If one measures an angular distribution at $E\neq E_R$, then

$$S=S^{OM}+e^{2i(\delta_{OM}+\phi+\pi/2+tg^{-1}2x)}\frac{a}{(1+4x^2)^{1/2}}\delta_{l,l_R}, \tag{3}$$

with $x=(E-E_R)/\Gamma$ and $a=2D/\Gamma$.

For the calculations, the optical model code ATHREE (Ref. 20) was modified to include up to two resonances. The following procedure was used in fitting the data. At first the data in the forward angles region were used ($\theta_{c.m.}\leq 60°$) to determine the parameters of the Woods-Saxon optical potential with the additional requirement that the potential would not show a backward rise, as expected for a strongly absorbing potential. The parameters obtained for each angular distribution are given in Table II. The forward angle data seem to require slightly different potentials, even for the angular distributions measured at $E_{c.m.}=24.2$ and 24.7 MeV. The value of $a=2D/\Gamma$ was chosen to fit the value of the cross section at large angles. Neglecting possible contributions from elastic α particle transfer (see the following), the shape of the angular distribution in the backward angles region determines the l value of the resonating partial wave. The resonance mixing phase ($\theta=\phi$ on resonance and

TABLE I. Channel-channel cross correlation coefficients $C_{ij}(\Delta,\epsilon=0)$ [see Eq. (1)] for $^{16}O+^{20}Ne$ at two angles in three different exit channels. The averaging interval is set at $\Delta=1.2$ MeV, as discussed in the text. The finite range of the data yields an estimated error (Ref. 4), as given in parentheses.

		$\theta_{lab}=17°$			$\theta_{lab}=27°$		
	i/j	0^+	2^+	4^+	0^+	2^+	4^+
	2^+	0.38(0.09)					
17°	4^+	0.43(0.07)	0.33(0.03)				
	0^+	0.02(0.20)	−0.16(0.09)	−0.02(0.07)			
27°	2^+	0.44(0.09)	0.48(0.04)	0.33(0.03)	−0.06(0.09)		
	4^+	0.02(0.07)	−0.10(0.03)	0.32(0.02)	0.16(0.07)	−0.10(0.03)	

TABLE II. Optical model parameters.[a]

$E_{c.m.}$ (MeV)	V_0 (MeV)	R_0 (fm)	a (fm)	W_0 (MeV)	R_0^I (fm)	a (fm)
24.5[b]	60	1.113	0.617	60	1.005	0.739
17.4	55	1.194	0.638	35	1.230	0.515
18.5	22	1.070	0.974	30	1.230	0.515

[a]From forward angle fit. Used $R_0^{Coul}=1.0$ fm.
[b]For both 24.2 and 24.7 MeV angular distributions.

$\theta=\phi+tg^{-1}2x$ "off resonance") is adjusted to fit the angular distribution at the intermediate angles region where background and resonance terms interfere.

The following results were obtained: The two angular distributions at $E_{c.m.}=24.2$ and 24.7 MeV are consistent with a resonance in partial wave $l=17$, as can be seen in Fig. 8. The two angular distributions are markedly different only in the intermediate angles region. This implies in that scheme a "fast" change in the phase of the resonance. It is difficult to follow the change in that phase from just two angular distributions, but an obvious increase in the phase can be observed. Contributions from the elastic transfer process could be the reason for the deviations observed in the backward angles region.

At $E_{c.m.}=17.4$ MeV a 12^+ resonance is consistent with the data, as can be seen from Fig. 9. In that low energy region the optical model "background" amplitude contributes significantly and other l values could fit the data, too. As shown in Fig. 9, the $l=12$ $\phi=0°$ parameters combination yields the best fit to the data. The resonance parameters are given in Table III. Both resonating l values (12 and 17) are close to the value of the grazing partial wave (in the entrance channel), defined as the l value at which the optical model transmission coefficient is equal to $\frac{1}{2}$. In both cases the poorly known background amplitude yields an uncertainty in the dominant l value, with the error being $\Delta l=\pm 1$. Reaction data[10] yield dominance of the $l=18$ partial wave for the 24.5 MeV structure.

For the angular distributions measured at $E_{c.m.}=18.5$ MeV we note that the data are inconsistent with the assumption of a single resonance superimposed on a smooth background (see Fig. 10). The irregular angular distribution resembles an interference between more than one partial wave. To further study this distribution, the presence of two dominating l values was assumed. The first resonance was taken to be in the $l=12$ grazing partial wave at 17.4 MeV. In that case we were able to get a reasonable fit only with a mixture of $J^\pi=12^+$ and 8^+ resonances, as can be seen in Fig. 10. With the value of the phase and

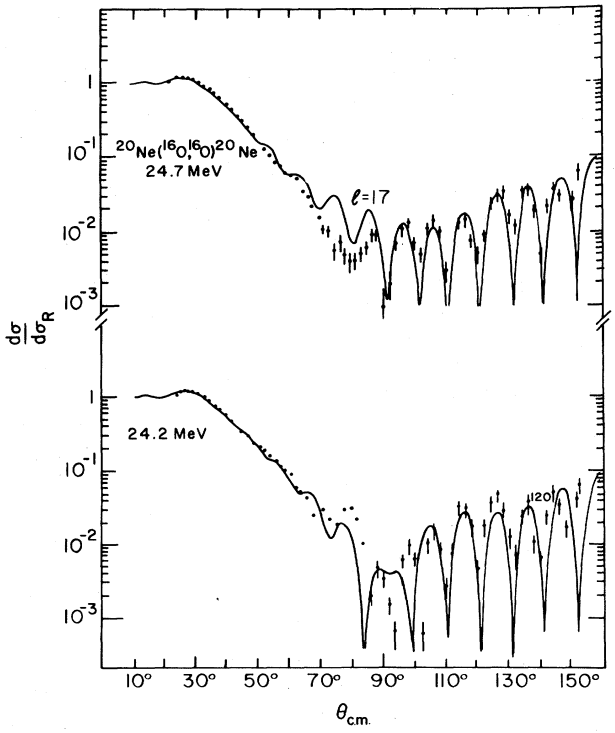

FIG. 8. Angular distribution predicted by the optical model plus resonance scheme. In the inset we show fits resulting from different mixing phase angles (for details, see the text).

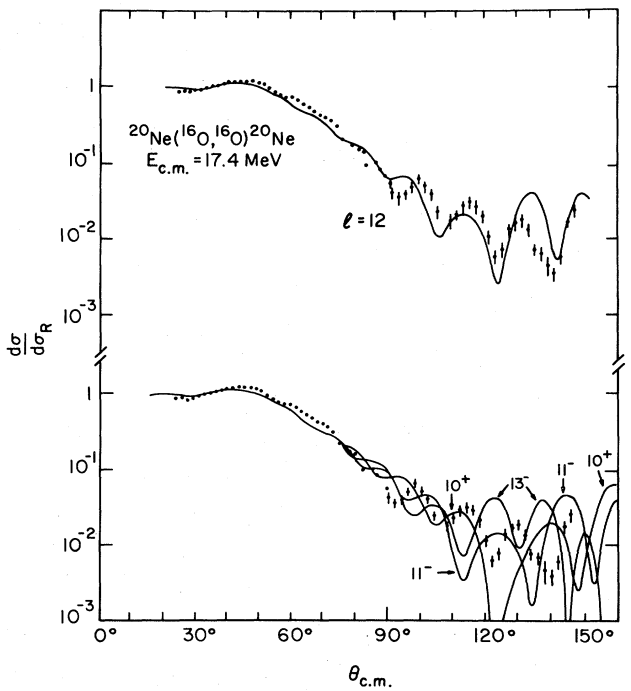

FIG. 9. As for Fig. 8.

TABLE III. Resonance parameters.

$E_{c.m.}$ (MeV)	l_1	a_1	$2\theta_1$	l_2	a_2	$2\theta_2$
24.2	17	0.22	20°			
24.7	17	0.22	120°			
17.4	12	0.22	0°			
18.5	12[a]	0.20	80°	8	0.17	0°

[a]First resonance energy is fixed to 17.4 MeV.

resonance parameters fixed for the 12^+ resonance at 17.4 MeV, a parameter space scan was performed for the second resonance. Two different choices of optical model potentials were tried, too. As can be seen in Fig. 10, only the 12+8 combination results a reasonable fit to the data. The data are thus consistent with an 8^+ resonance at $E_{c.m.}=18.5$ MeV. Such an assignment is also consistent with the absence of a structure at $\theta_{c.m.}=146°$, close to a zero of P_8 at $\theta_{c.m.}\simeq 144°$. We note that such an occurrence of interference of the grazing partial wave with $J^\pi=8^+$ resonances was pointed out[13] for a particular family of resonances in many different heavy ion systems, including the $^{16}O+^{20}Ne$ system. We refer the reader to Ref. 13 where the significance of such ubiquitous occurrences is discussed.

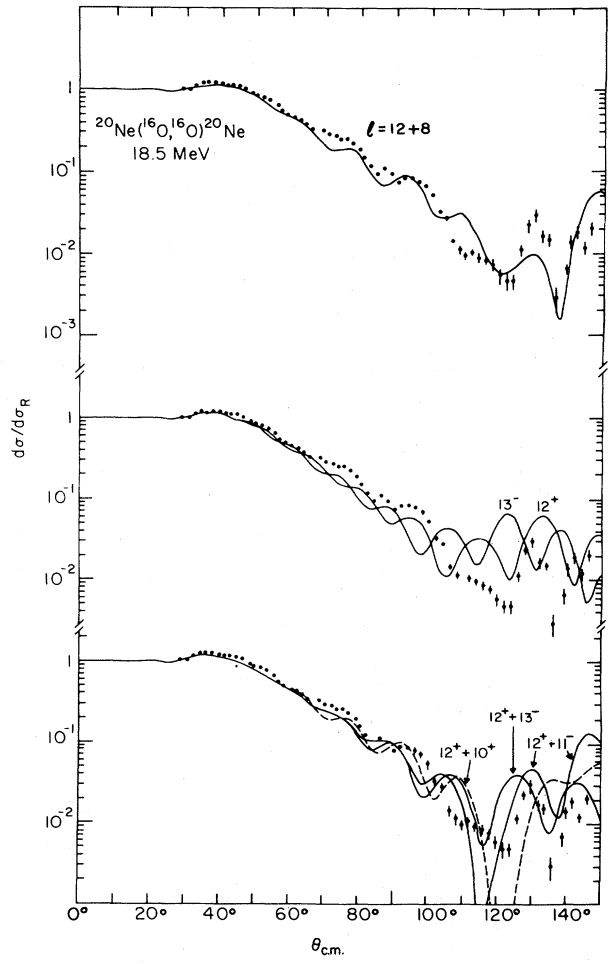

FIG. 10. Angular distributions predicted by the optical model plus one and two resonances. Several best fits with a single l are shown, as well as several combinations of two interfering l values, as discussed in the text.

C. "The elastic transfer" mechanism

The nucleus ^{20}Ne has a large fractional parentage[21] to an $\alpha+^{16}O$ structure, and a small threshold for α particle emission ($E_B=4.73$ MeV). These two effects together imply that the amplitude of the type $^{20}Ne(^{16}O,^{20}Ne)^{16}O$—describing an α particle transfer between identical cores—could possibly play an important role in the elastic scattering of $^{16}O+^{20}Ne$. Thus we write the scattering amplitude as

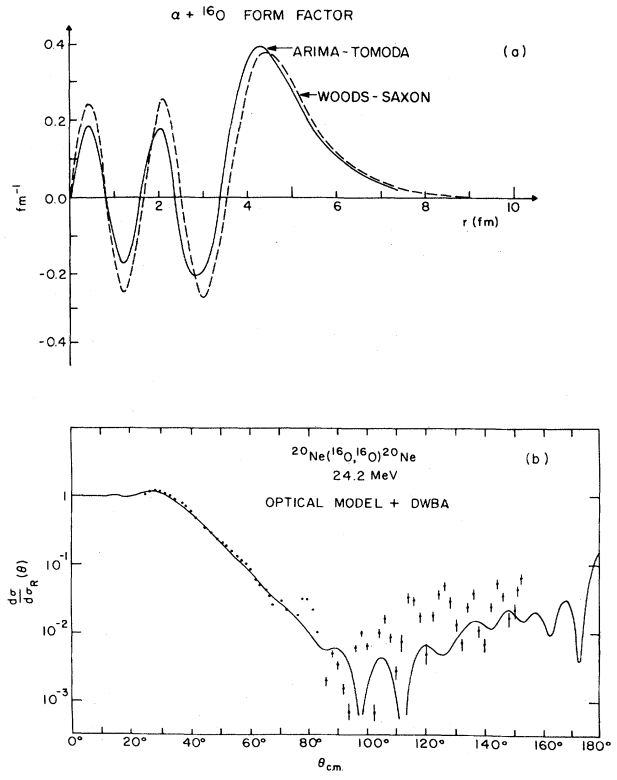

FIG. 11. Angular distribution calculated as a coherent sum of elastic and DWBA α transfer amplitudes. The DWBA form factor parameters are taken from the theoretical calculation of Ref. 21. The microscopic form factor is shown [in part (a)] and discussed in the text. No other adjustable parameters are used. The elastic transfer process is important at the far backward angles region but cannot explain the resonancelike structure.

$$f(\theta)=f_{\rm el}^{\rm dir}(\theta)+f^{\rm transfer}(\pi-\theta)\ , \tag{4}$$

where $f(\theta)$ is the total scattering amplitude, $f_{\rm el}^{\rm dir}$ is the optical model elastic amplitude, and $f^{\rm transfer}(\pi-\theta)$ is the single step direct DWBA α particle transfer amplitude to center of mass angle $\pi-\theta$. The second amplitude is an exchange amplitude that arises from the antisymmetrization. It is calculated in the DWBA approximation with recoil effects being treated exactly[22] and with a potential of a finite range.

The bound state form factor used in the DWBA calculations was calculated by solving the Schrödinger equation (for $E_B=4.729$ MeV) with a Woods-Saxon potential. The radius of the potential was chosen to be $R=1.4\times A^{1/3}$ ($A=16$), in order to reproduce the exponential decay of the microscopic wave function of Tomoda-Arima[21] for large radii, and the diffusivity of the well was fixed at $a=0.65$ fm. The number of nodes was taken to be four. The depth of the potential was varied until a solution was obtained at $V_0=110.6$ MeV. The resultant bound state wave function is shown in Fig. 11. In the same figure we show the microscopic wave function calculated in Ref. 21. At large radii the two wave functions are nearly identical and have the same normalization.

In the cluster model the differential cross section factorizes according to

$$(d\sigma/d\Omega)^{\rm expt}=S_{\rm in}S_{\rm out}(d\sigma/d\Omega)^{\rm DWBA}\ , \tag{5}$$

where $S_{\rm in}=S_{\rm out}$ is the α particle spectroscopic factor for ^{20}Ne.

The calculations of the scattering amplitude were performed using the computer code LOLA (Ref. 23). The code was modified to yield a coherent sum of the elastic and DWBA amplitudes calculated at $\pi-\theta$ and multiplied by the spectroscopic factor. The spectroscopic factor was chosen to be $S=0.32$ in order to yield the alpha spectroscopic amplitude (given by $\sqrt{S}\,\phi_{\rm WS}$) of the theoretical wave function, as seen in Fig. 11. This value is close to the one predicted by theory, $S=0.21$ (Ref. 21).

The calculations were done for all measured angular distributions. In Fig. 11 we show the calculations at $E_{\rm c.m.}=24.2$ MeV. The results of these calculations were confirmed with equivalent calculations using the code PTOLEMY (Ref. 24). Aside from the above theoretical input, no adjustable parameters exist in these calculations. The absolute value of the cross section at backward angles is not fitted by these calculations and neither is the oscillatory pattern. However, they indicate a large contribution at the very far backward angles region of the elastic transfer amplitude, in accordance with the conclusions of Ref. 15.

V. CONCLUSION

We have studied the energy and angular dependence of the scattering of ^{16}O from ^{20}Ne. Structures typical of light heavy ion scattering were found. The data presented here do not require the existence of resonances, but are consistent with a resonance interpretation. The importance of the elastic transfer, in the far backward angle region, was demonstrated.

We wish to thank the support staff of the A. W. Wright Nuclear Structure Laboratory at Yale, especially R. Bonito, L. Bakkum, and S. Sicignano, for a careful preparation of the manuscript and figures of this paper.

*Present address: A. W. Wright Nuclear Structure Laboratory, Yale University, New Haven, CT 06511.

†Present address: Cyclotron Institute, Texas A&M University, College Station, TX 77843.

‡Permanent address: AT&T Bell Laboratories, Naperville, IL 60540.

§Present address: Massachusetts Institute of Technology, Department of Physics, Cambridge, MA 02139.

**Present address: Lawrence Berkeley Laboratory, Berkeley, CA 94720.

††Permanent address: Bundesministerium fur Forschung und Technologie, Bonn, Federal Republic of Germany.

[1]See, e.g., A. Gobbi and D. A. Bromley, in *Heavy Ion Collisions,* edited by R. Bock (North-Holland, Amsterdam, 1979), Vol. I, p. 485; P. Braun-Munzinger, Nucl. Phys. **A409**, 31C (1983).

[2]J. V. Maher, M. W. Sachs, R. H. Siemssen, A. Weidinger, and D. A. Bromley, Phys. Rev. **188**, 1665 (1969).

[3]W. Scheid, W. Greiner, and R. Lemmer, Phys. Rev. Lett. **25**, 176 (1970).

[4]M. L. Halbert, F. E. Durham, and A. Van der Woude, Phys. Rev. **162**, 899 (1967); D. Shapira, R. G. Stokstad, and D. A. Bromley, Phys. Rev. C **10**, 1063 (1974); J. P. Bondorf, Nucl. Phys. **A202**, 30 (1973).

[5]A. Richter and C. Toepffer, see Ref. 1, p. 1.

[6]P. Braun-Munzinger, G. M. Berkowitz, T. M. Cormier, C. M. Jachcinski, J. W. Harris, J. Barrette, and M. J. LeVine, Phys. Rev. Lett. **38**, 944 (1977); J. Barrette, M. J. LeVine, P. Braun-Munzinger, G. M. Berkowitz, M. Gai, J. W. Harris, and C. M. Jachcinski, *ibid.* **40**, 445 (1978); Phys. Rev. C **24**, 1010 (1981); P. Braun-Munzinger and J. Barrette, Phys. Rep. **87**, 209 (1982).

[7]M. R. Clover, R. M. Devries, R. Ost, N. J. A. Rust, R. N. Cherry, Jr., and H. E. Gove, Phys. Rev. Lett. **40**, 1008 (1978); R. Ost, M. R. Clover, R. M. Devries, B. R. Fulton, H. E. Gove, and N. J. Rust, Phys. Rev. C **19**, 740 (1979).

[8]R. R. Betts, S. B. Dicenzo, and J. F. Peterson, Phys. Lett. **100B**, 117 (1981); R. R. Betts, B. B. Back, and B. G. Glagola, Phys. Rev. Lett. **47**, 23 (1981).

[9]M. M. Fowler and R. C. Jared, Nucl. Instrum. Methods **124**, 341 (1975).

[10]J. Schimizu, W. Yokota, T. Nakagawa, Y. Fukuchi, H. Yamaguchi, M. Sato, S. Hanashima, Y. Nagashima, K. Furuno, K. Katori, and S. Kubono, Phys. Lett. **112B**, 323 (1982).

[11]The data of the authors of Ref. 10 are shown and analyzed in Y. Kondo, B. A. Robson, and R. Smith, Nucl. Phys. (in press).

[12]J. Barrette, P. D. Bond, M. J. LeVine, and I. Tserruya, Bull.

Am. Phys. Soc. **24**, 570 (1979); see also Figs. 2—11 of Ref. 6; Phys. Rep. **87**, 209 (1982).

[13]M. Gai, E. C. Schloemer, J. E. Freedman, A. C. Hayes, S. K. Korotky, J. M. Manoyan, B. Shivakumar, S. M. Sterbenz, H. Voit, S. J. Willett, and D. A. Bromley; Phys. Rev. Lett. **47**, 1878 (1981); M. Gai and D. A. Bromley (unpublished).

[14]M. A. Xapsos, P. A. De Young, L. J. Satkowiak, and J. J. Kolata, Phys. Rev. C **25**, 2457 (1982).

[15]R. Stock, U. Jahnke, D. L. Hendrie, J. Mahony, C. F. Maguire, W. F. W. Schneider, D. K. Scott, and G. Wolschin, Phys. Rev. C **14**, 1824 (1976).

[16]R. Vandenbosch, M. P. Webb, and M. S. Zisman, University of Washington report, 1975, p. 122 (unpublished).

[17]G. Pappalardo, Phys. Lett. **13**, 320 (1964).

[18]A. Richter, in *Nuclear Spectroscopy and Reactions,* edited by J. Cerny (Academic, New York, 1974), Vol. B, p. 343.

[19]C. A. Engelbrecht and H. A. Weidenmuller, Phys. Rev. C **8**, 859 (1973).

[20]E. H. Auerbach, Comp. Sci. Comm. **15**, 165 (1978).

[21]T. Tomoda and A. Arima, Ref. 31 in A. Arima, *Proceedings of the International Conference on Nuclear Physics, Munich, 1973* (North-Holland, Amsterdam, 1973), p. 183.

[22]R. M. Devries, Phys. Rev. C **8**, 951 (1973).

[23]R. M. Devries, University of Rochester report, 1974 (unpublished).

[24]M. H. MacFarlane and S. C. Pieper, computer code PTOLMEY, Argonne National Laboratory Report ANL-76-11, Rev. 1 (unpublished).